THE JOURNAL OF BIOLOGICAL CHEMISTRY
Vol. 277, No. 1, Issue of January 4, pp. 735–745, 2002

Printed in U.S.A.

Structure-Function Analysis of the Heat Shock Factor-binding Protein Reveals a Protein Composed Solely of a Highly Conserved and Dynamic Coiled-coil Trimerization Domain*

Received for publication, September 6, 2001, and in revised form, October 17, 2001
Published, JBC Papers in Press, October 25, 2001, DOI 10.1074/jbc.M108604200

Li-Jung Tai‡§¶, Sally M. McFall‡§‖, Kai Huang‡, Borries Demeler‡‡, Sue G. Fox‡§, Kurt Brubaker‡, Ishwar Radhakrishnan‡§§, and Richard I. Morimoto‡§¶¶**

*From the ‡Department of Biochemistry, Molecular Biology, and Cell Biology, the §Rice Institute for Biomedical Research, and the **Structural Biology NMR Facility, Northwestern University, Evanston, Illinois 60208 and the ‡‡Center for Analytical Ultracentrifugation of Macromolecular Assemblies, Department of Biochemistry, University of Texas Health Science Center, San Antonio, Texas 78284-7760*

Heat shock factor-binding protein (HSBP) 1 is a small, evolutionarily conserved protein originally identified in a yeast two-hybrid screen using the trimerization domain of heat shock factor (HSF) 1 as the bait. Similar in size to HSF1 trimerization domain, human HSBP1 contains two arrays of hydrophobic heptad repeats (designated HR-N and HR-C) characteristic of coiled-coil proteins. Proteins of the HSBP family are relatively small (<100 residues), comprising solely a putative coiled-coil oligomerization domain without any other readily recognizable structural or functional motif. Our biophysical and biochemical characterization of human HSBP1 reveals a cooperatively folded protein with high α-helical content and moderate stability. NMR analyses reveal a single continuous helix encompassing both HR-N and HR-C in the highly conserved central region, whereas the less conserved carboxyl terminus is unstructured and accessible to proteases. Unlike previously characterized coiled-coils, backbone ^{15}N relaxation measurements implicate motional processes on the millisecond time scale in the coiled-coil region. Analytical ultracentrifugation and native PAGE studies indicate that HSBP1 is predominantly trimeric over a wide concentration range. NMR analyses suggest a rotationally symmetric trimer. Because the highly conserved hydrophobic heptad repeats extend over 60% of HSBP1, we propose that HSBP most likely regulates the function of other proteins through coiled-coil interactions.

Protein oligomerization is a general mechanism for regulating and mediating diverse cellular processes including cytoskeletal interaction and cell motility, transcriptional activation, membrane trafficking, and intracellular signaling. A fundamental oligomerization motif is the "coiled-coil," which modulates protein structure and dynamics through its ability to mediate homotypic as well as heterotypic associations (for reviews of coiled-coils, see Refs. 1 and 2). Prominent examples of coiled-coil proteins include desmin and keratins forming the rigid framework of intermediate filaments (3), mannose-binding protein involved in antibody-independent immune response (4), Jun and Fos heterodimerizing to activate transcription (5), and the heat shock transcription factor 1 (HSF1)[1] oligomerizing temporally upon stress activation (6, 7). Because of its central role in biology and also because of its apparent simplicity, the coiled-coil motif has evoked considerable interest as a biological motif and as a paradigm for studies of protein folding (8–10) and *de novo* protein design (11, 12).

The coiled-coil structural motif comprises two or more right-handed α-helices wrapped around each other with a small, left-handed superhelical twist (13). The hallmark of coiled-coils at the primary structure level is a seven-residue repeating sequence termed the heptad repeat in which the first and fourth residues (*i.e.* **a** and **d** in the sequence **abcdefg**) typically occupy the interhelical interface and are generally hydrophobic. Extensive structural and thermodynamic analyses of native and model coiled-coils have revealed that the shape and packing of the **a** and **d** residues determine, to a large extent, the stability and the preferred oligomerization state of the coiled-coils whereas the **e** and **g** residues, which are generally bulky, polar, or charged, contribute toward specificity and establishment of the proper chain register positions (9, 14–27). Despite these advances in our understanding, reliable predictions of the preferred oligomerization state as well as packing of individual subunits remains a challenge for many naturally occurring coiled-coils.

Heat shock-binding protein 1 (HSBP1) is a 76-residue acidic protein that was isolated from a yeast two-hybrid screen using the coiled-coil containing trimerization domain of heat shock

* This work was supported in part by National Institutes of Health Grant GM38109 and a grant from the Carol and Marvin Gollob Foundation (both to R. I. M.) and by a grant from the Searle Leadership Fund provided by the Chicago Community Trust (to I. R.). Funds for upgrading the 600-MHz NMR spectrometer at Northwestern University were provided in part by the National Institutes of Health. Support for the development of sedimentation analysis software was provided by National Science Foundation Grant DBI-9974819 (to B. D.). The costs of publication of this article were defrayed in part by the payment of page charges. This article must therefore be hereby marked "*advertisement*" in accordance with 18 U.S.C. Section 1734 solely to indicate this fact.

¶ Supported by National Institutes of Health NIGMS Medical Scientist Training Program Fellowship GM08152.

‖ Supported by National Institutes of Health Signal Transduction and Cancer Training Grant 5T32CA70085-03 and NRSA Fellowship F32 GM20246-01.

§§ To whom correspondence may be addressed. Tel.: 847-467-1173; Fax: 847-467-6489; E-mail: i-radhakrishnan@northwestern.edu.

¶¶ To whom correspondence may be addressed. Tel.: 847-491-3340; Fax: 847-491-4461; E-mail: r-morimoto@northwestern.edu.

[1] The abbreviations used are: HSF1, heat shock transcriptional factor 1; CD, circular dichroism; CPMG, Carr-Purcell-Meiboom-Gill technique; HR-N, amino-terminal hydrophobic heptad, HR-C, carboxyl-terminal hydrophobic heptad; HSBP1, heat shock factor-binding protein 1; HSQC, heteronuclear single quantum coherence; NOESY, nuclear Overhauser effect spectroscopy; rpm, rotations per minute; SEC, size exclusion chromatography; T_m, midpoint of thermal denaturation; θ_{222}, molar ellipticity per residue at 222; PBS, phosphate-buffered saline; NOE, nuclear Overhauser effect; TROSY; transverse relaxation optimized spectroscopy.

transcription factor HSF1 as the bait (28). Yeast two-hybrid assays with HSBP1 as both bait and prey indicate that HSBP1 self-associates (Ref. 28, and see below). HSBP1 is highly conserved in a wide variety of organisms but has no readily identifiable homologues in the repository of experimentally determined high resolution structures in the Research Collaboratory for Structural Bioinformatics Protein Data Bank (www.rcsb.org). Sequence analysis suggested a highly helical protein with two tandem arrays of heptad repeat devoid of other readily recognizable structural motif(s).

These attributes of the HSBP protein family led us to characterize the biochemical and biophysical properties of human HSBP1. Here, we show that HSBP1 is an evolutionarily conserved protein that exists as a highly helical, homotrimeric coiled-coil with the individual subunits arranged in a parallel and unstaggered manner relative to each other. Although coiled-coil proteins are relatively common, to our knowledge, HSBP1 is the first protein that has been described that is composed solely of a coiled-coil domain. Thus, the HSBP protein family may represent a new, structurally distinct subtype of coiled-coils and can serve as a model for understanding the structural principles of coiled-coils.

EXPERIMENTAL PROCEDURES

Cloning—Human wild-type HSBP1 and the COOH-terminal truncation mutant HSBP1 65Δ were PCR-amplified with *Pfu* DNA polymerase (Stratagene). For wild-type HSBP1, the amino- and carboxyl-terminal primers are 5′-ATG GCC GAG ACT GAC CCC AAG ACC G-3′ and 5′-TTC CGC TCG AG T CAA CTC TTT TGC GTG GC-3′, respectively. The primer for the carboxyl terminus of HSBP1 65Δ (65Δ-C) is 5′-TTC CGC TCG AGT CTT CCA GTT CTT CCA CCC C-3′ (Invitrogen). The PCR products were cloned into the multiple cloning site immediately 3′ of the glutathione *S*-transferase gene in pET-42a(+) (Novagen) expression vector, which was linearized with *Psh*AI and *Xho*I. Sequences of the constructs were confirmed by automated sequencing in both forward and reverse directions. The wild-type HSBP1 lacks the amino-terminal methionine. There are no extra amino acids derived from the vector.

Yeast Two-hybrid Interaction Assay—The *Eco*RI-*Xho*I fragment containing the canine HSBP1 cDNA from pJG4-5 was cloned into the *Eco*RI-*Sal*I site of pEG202 to form pEG202-cHSBP1 (28). pJG4-5-HSBP1 65Δ was generated by PCR using a primer specific to pJG4-5 (JG45P, 5′-CTC TTG CTG AGT GGA GAT-3′) and an HSBP1-specific primer, 65Δ-C. The fragment was restricted with *Eco*RI and *Xho*I and inserted into the *Eco*RI-*Xho*I site of pJG4-5 and confirmed by sequencing. The pEG202 plasmids (LexA fusions) were transformed into EGY48 containing pSH18–34 *lacZ* reporter plasmid (gift of R. Brent). The pJG4-5 plasmids (activation domain fusions) were transformed into R3159 (gift of R. Gaber). The strains were mated overnight on YPD medium and replica-plated onto galactose-containing dropout medium lacking histidine, tryptophan, and uracil and supplemented with 5′-bromo-4-chloro-3-indoyl-β-D-galactopyranoside (29). β-Galactosidase assays were performed by the method of Miller (30). Activity was expressed as relative activity with wild-type pEG202-cHSBP1 *versus* wild-type pJG4-5-cHSBP1 set arbitrarily as 100%.

Protein Overexpression and Purification—Escherichia coli strain BL21(DE3) harboring pET-42a(+)-HSBP1 plasmid was grown in LB medium to A_{600} of 0.9 and then induced with 1 mM isopropyl-β-D-thiogalactopyranoside for 3 h. Cells were harvested through centrifugation, and the bacterial pellet was re-suspended and freeze-thawed three times in 1× PBS (140 mM NaCl, 3 mM KCl, 1 mM KH_2PO_4, 8 mM Na_2HPO_4) with protease inhibitors (2.5 μg/ml pepstatin A, 2.5 μg/ml leupeptin, 2.5 μg/ml antipain, 2.5 μg/ml chymostatin, and 1 mM phenylmethylsulfonyl fluoride). The suspension was sonicated, and Triton X-100 was added to a final concentration of 1% before the suspension was centrifuged for 30 min at 32,000 × *g*. The supernatant was loaded onto a glutathione-Sepharose column for affinity chromatography. The column was then washed with 20 column volumes of 1× PBS, followed by 10 column volumes of buffer containing 150 mM NaCl, 50 mM Tris, pH 7.5. Overnight on-column cleavage with factor Xa at 1:300 w/w factor Xa:substrate ratio (New England Biolabs) was carried out at room temperature while nutating in 150 mM NaCl, 2 mM $CaCl_2$, 50 mM Tris, pH 7.5. The eluent was further purified via reverse phase high pressure liquid chromatography using a Vydac C18 column, equilibrated with 48.8% acetonitrile, 0.1% trifluoroacetic acid. A linear 0.5% acetonitrile/min gradient was used to fractionate proteins. The identity and purity of the samples were confirmed by electrospray ionization mass spectrometry (Analytical Services Laboratory, Northwestern University, Chicago, IL). Protein concentrations were measured by amino acid analysis (Protein Research Laboratory, University of Illinois, Chicago, IL). These measurements were used to calculate extinction coefficients.

Monoclonal Antibody—A monoclonal antibody against human HSBP1 was made following standard protocols (31). Briefly, 50 μg of purified, recombinant HSBP1 was injected intraperitoneally into each mouse with equal volume of Titermax (CytRx Co.) every 3 weeks. Tail bleeds were screened by enzyme-linked immunosorbent assay. Mice with positive enzyme-linked immunosorbent assay were intravenously injected with ~35 μg of antigen in PBS and sacrificed 3 days later. Splenocytes were harvested and fused with myeloma Sp2/O-Ag14. Hybridoma were selected and screened to monoclonality. Specificity of the monoclonal antibody 12F9 was confirmed by immunoprecipitation and Western blot analysis in the presence of competitors.

Circular Dichroism Spectroscopy—Circular dichroism spectra were recorded on a Jasco J-715 spectropolarimeter equipped with a computer-controlled Peltier device and water bath for temperature control. The measurement wild-type HSBP1 were performed at 17 μM in 20 mM NaCl, 1 mM EDTA, 5 mM sodium phosphate buffer, pH 7. For wavelength scans, spectra were recorded at 20 °C from 260 to 190 nm at a scan rate of 5 nm/min. Temperature scans for thermal denaturation and renaturation studies were performed at 222 nm wavelength at a scan rate of 30 °C/h. Data have been corrected for the base lines by subtracting the data from buffer. The measured ellipticity was converted to molar ellipticity ($[\theta]$), which is independent of concentration and the number of residues in the protein. Molar ellipticity at 222 nm was used to estimate helical content using the relation $(-\theta_{222} + 2340)/30{,}300$ (32).

Limited Proteolysis—Wild-type HSBP1 was pre-incubated in 100 mM NH_4HCO_3 for 15 min at 30 °C. Trypsin (Sigma) or V8 (Sigma) proteases were added at enzyme to substrate w/w ratios of 1:33.3 and 1:100, respectively. Proteolysis was performed for 30 min at 30 °C, after which the solution was mixed with an equal volume of acetonitrile and flash-frozen in a methanol/dry ice bath. The samples were lyophilized, re-suspended in 50% acetonitrile, and analyzed by electrospray ionization mass spectrometry (Analytical Services Laboratory, Northwestern University).

NMR Sample Preparation—Uniformly ^{15}N-labeled wild-type HSBP1 and ^{15}N-^{2}H, ^{15}N- and ^{2}H, ^{13}C,^{15}N-labeled HSBP1 65Δ were produced by growing transformed *E. coli* in M9 minimal media containing ^{15}N-ammonium sulfate (Cambridge Isotopes) and D-glucose (or [$^{13}C_6$]D-glucose (Isotec) or [$^{2}H_7$,$^{13}C_6$]D-glucose (Martek)) as the sole nitrogen and carbon sources, respectively. All labeled proteins were produced in a fermenter following the strategy outlined by Cai *et al.* (33). Perdeuterated proteins were expressed either in 15% H_2O, 85% $^{2}H_2O$ or in 99.8% $^{2}H_2O$ (Isotec). The extent of isotope incorporation was assessed by mass spectrometry (typically, 98% for ^{13}C and ^{15}N, and 80 and 95% for ^{2}H in the ^{2}H, ^{15}N- and ^{2}H, ^{13}C, ^{15}N-labeled HSBP1 65Δ samples, respectively). NMR samples were prepared in the concentration range 0.6–1.2 mM in 90% H_2O, 10% $^{2}H_2O$ buffer (20 mM $^{2}H_{11}$-Tris $^{2}H_4$-acetate, pH 6.0, 50 mM NaCl, 0.2% (w/v) NaN_3).

All NMR experiments were performed on a Varian Inova 600-MHz spectrometer at 40 °C. NMR data processing and analysis were performed using Felix 98 software (Molecular Simulations) modified to include the StripTool interface (34). Backbone ^{1}H and ^{15}N resonances for residues at the amino and carboxyl termini of full-length HSBP1 were assigned from three-dimensional ^{15}N-edited NOESY-HSQC (mixing time, τ_m = 100 ms) and total correlation spectroscopy-HSQC (τ_m = 60 ms) spectra. $^{1}H^{N}$, $^{13}C^{\alpha}$, $^{13}C^{\beta}$, $^{13}C'$, and ^{15}N resonances for HSBP1 65Δ were assigned from three-dimensional HNCA, HN(CO)CA, HNCACB, HN(CA)CB, HN(COCA)CB, HNCO (35, 36), and ^{15}N-edited NOESY-TROSY (τ_m = 200 ms) (37) spectra. Pulse sequences were modified to incorporate the TROSY principle (38, 39) for enhanced sensitivity. Deuterium decoupling was applied during the periods when transverse carbon magnetization was present in the HNCA, HN(CO)CA, and HNCACB experiments. Excluding the methionine at the amino terminus, all backbone $^{1}H^{N}$, ^{15}N, $^{13}C^{\alpha}$, $^{13}C^{\beta}$, and $^{13}C'$ resonances were assigned except ^{15}N and $^{1}H^{N}$ of Ala-2, $^{13}C'$ of Asp-5 and Glu-65.

To assess internal dynamics, ^{15}N spin relaxation parameters were measured for backbone amides of HSBP1 65Δ. (^{1}H)-^{15}N heteronuclear NOE measurements (40) were performed in quadruplicate using the ^{2}H,^{15}N-labeled HSBP1 65Δ sample with the recycle delay set to 3 s. ^{15}N spin-lattice relaxation rate constants (R_1) were measured using the

pulse sequence described by Farrow *et al.* (40) with parametric relaxation delays (T) set to 40, 200, 400, 800, 1200, 1800, 2400, 3000, and 5000 ms. Duplicate spectra for T = 40 and 1800 ms were recorded for estimating experimental error. ^{15}N spin-spin relaxation rate constants (R_2) were evaluated using a TROSY-CPMG pulse sequence (41) on the ^{2}H,^{13}C,^{15}N-labeled sample of HSBP1 65Δ. ^{15}N R_2 measurements were performed using two different CPMG delays, τ_{cp} = 0.8 and 5 ms, to evaluate chemical exchange contribution to the effective transverse relaxation time constant R_2*. For τ_{cp} = 0.8 ms, spectra were recorded with T set to 3.2, 9.6, 19.2, 32.0, 41.6, 60.8, 80.0, 102.4, 160, and 198.4 ms. Duplicate spectra were recorded for T = 19.2 and 102.4 ms. For τ_{cp} = 5 ms, spectra were recorded with T set to 20, 40, 60, 80, 100, 160, and 200 ms. Duplicate spectra were recorded for T = 20 and 100 ms. A home-written Felix macro was used to optimize and extract peak intensities. The *cpmgr2* (42) program was used to fit the peak intensity data to a two-parameter exponential function for obtaining ^{15}N R_1 and R_2 values for each residue. Uncertainties in peak intensities were estimated from duplicate measurements and propagated into the measured R_1, R_2, and NOE values.

Size Exclusion Chromatography—Approximately 100 μl of wild-type HSBP1 ranging from 5 to 500 μM starting concentration was injected into a Superdex 75 HR analytical column (Amersham Biosciences, Inc.). These experiments were performed at room temperature under the following buffer conditions: 150 mM NaCl, 50 mM sodium acetate, 2 mM $MgCl_2$, 2 mM $CaCl_2$, 0.2 mM $ZnCl_2$, pH 4.5, 100 mM NaCl, 50 mM imidazole, pH 7, 100 mM NaCl, 5 mM $CaCl_2$, 50 mM Tris, pH 8. Protein standards (Amersham Biosciences, Inc.) were run immediately before each run, and the samples were monitored at 230, 260, and 280 nm. One-milliliter fractions were collected, and the location of the protein was confirmed by Western blot analysis. The apparent molecular weight and Stokes radius of HSBP1 was calculated for each run from the graphs of the logarithm of the molecular weights and of Stokes radii as functions of elution profiles (K_{av}) of the protein standards (43).

Native Polyacrylamide Gel Electrophoresis—Wild-type HSBP1 and 65Δ were mixed in 1:1 ratio at a total concentration of 60 μM and incubated at either 60, 80, or 90 °C for 5 min followed by incubation at 37 °C for 15 min. Alternatively, an incubation time course of the two proteins was performed at room temperature from 5 min to overnight. SDS-free loading dye was added so that final protein concentration ranged from 0.5 to 12 μM was loaded and resolved on discontinuous Tris-glycine SDS-free polyacrylamide gels (44) at either room temperature or 4 °C. Alternatively, 0.5× TBE or 1× TBE gels were used at either temperatures. The gel was transferred and blotted with 12F9, a monoclonal antibody against HSBP1, to detect homo- and hetero-oligomers of HSBP1.

Sedimentation Equilibrium Ultracentrifugation—Sedimentation equilibrium experiments of wild-type HSBP1 were performed using a two-sector aluminum centerpiece in a Beckman Coulter (Fullerton, CA) XL-A analytical ultracentrifuge with an 8-position An-50 Ti rotor in absorbance mode. Protein samples were dialyzed at 4 °C prior to the run for about 2 days with more than three changes (1×10^9 dilutions) of buffer (150 mM NaCl, 50 mM sodium phosphate, pH 7). The dialysate of each sample was used for making protein dilutions and also for the reference solution. 150 μl of sample with initial absorbances OD_{230} = 0.2–0.5 were loaded and sedimented to equilibrium at 20 °C at 15,000, 20,000, 25,000, 30,000, 35,000, 40,000, 45,000, and 50,000 rpm sequentially. Dual scans were acquired to confirm attainment of equilibrium. Scans at 230 nm were acquired in step mode with a radial step size of 0.001 cm down the axis of the cell, with 50 replicates at each step point. Data between 0.0 and 0.9 in optical density were global fitted using UltraScan 5.0 software (B. D., www.ultrascan.uthscsa.edu). Extinction coefficient profile, partial specific volumes, buffer density and viscosity corrections were calculated with the UltraScan software. Monte Carlo simulations for the monomer ↔ dimer model were performed on a 40-processor Beowulf system running Slackware Linux. Protein samples before and after sedimentation equilibrium looked identical on native gel (data not shown).

Sedimentation Velocity Ultracentrifugation—Sedimentation velocity studies of wild-type HSBP1 were performed using two-channel aluminum centerpieces on a Beckman Coulter XL-A analytical ultracentrifuge. Protein samples were dialyzed and prepared as described above. Experiments were performed at 23 °C and 60,000 rpm. Starting sample concentrations ranged from 5 μM to 1 mM. The rotor with protein sample was equilibrated in the centrifuge to 23 °C in vacuum before each run was started. Velocity data were collected in continuous scan mode with a step size of 0.001 cm at multiple wavelengths depending on the protein concentration. Data editing, van Holde-Weischet (45), and finite element (46) analyses were performed using UltraScan version 5.0. Sedimentation coefficients, diffusion coefficients, and molecular weights were corrected for water at 20 °C as reported by UltraScan.

RESULTS

HSBP1 Is Highly Conserved across Diverse Species—Human HSBP1 is a 76-residue, acidic protein that belongs to a highly conserved family of proteins present in diverse species. A sequence similarity search of the National Center for Biotechnology Information expressed sequence tags and "nonredundant" nucleotide sequence data bases using the human HSBP1 protein sequence revealed homologues, ranging in size from 74 to 99 residues, in more than 30 plant and animal species as well as fission yeast (47). In several plant species, including corn and rice, multiple homologues were found. Furthermore, comparing the intron-exon structures of known and putative genomic HSBP loci strengthens the hypothesis that these putative homologues belong to the same family. For example, the *Homo sapiens*, *Caenorhabditis elegans*, *Drosophila melanogaster*, *Arabidopsis thaliana*, and *Schizosaccharomyces pombe* HSBP loci share at least two successive intron-exon junctions between residues 15 and 16 of the human protein sequence (Fig. 1*A*), implying a common evolutionary origin.[2]

A sequence alignment of a subset of HSBP proteins from diverse species is shown in Fig. 1*A*. Within each of the plant and animal kingdoms, the sequence similarity is greater than 60% among HSBP homologues. Across the two kingdoms, however, the similarity drops to 50%. The *Schizosaccharomyces pombe* HSBP1 is the most distant member of the family, sharing only 30–46% sequence similarity with its plant and animal relatives. Expressed sequence tag data base searches further revealed that HSBP1 mRNA is ubiquitously expressed in a variety of murine and human normal and cancerous tissues and organs, including placenta, lung, liver, kidney, heart, testis, ovary, uterus, brain, adipose tissue, and white blood cells, as well as multiple organs and developmental stages in plant. Western blot analysis using monoclonal antibody 12F9 raised against human HSBP1 confirmed the ubiquitous expression of HSBP1 protein in all major mouse organs.[3] These results suggest that HSBP proteins have a fundamental role in diverse organisms and in a variety of animal and plant cell types.

HSBP1 Contains Two Regions of Hydrophobic Heptad Repeats—Analysis of HSBP1 sequences reveals that the carboxyl-terminal half of the protein (comprising residues 35–59 of human HSBP1 and designated "HR-C") follows an unambiguous heptad repeat pattern (Fig. 1*A*). A similar pattern can also be detected in the amino-terminal half of the protein (designated "HR-N"), although the presence of consecutive hydrophobic residues (for example, residues Val-15 and Val-16, and Leu-19 and Leu-20 in human HSBP1; Fig. 1*A*) introduces some ambiguity in assigning residues to the heptad positions. This was resolved by maximizing the number of highly conserved hydrophobic residues at **a** and **d** positions. However, this did not result in a continuous heptad repeat pattern extending from residues 10 to 59. Rather, a discontinuity in the heptad pattern occurs at residue 35 and can be characterized as a "stutter," which involves a deletion of three heptad positions (*i.e.* ***abcdefgaefgabcd***). Stutters have been noted in coiled-coil structures and are commonly associated with localized structural

[2] Accession numbers for these genes are as follows: *S. pombe*, NCB accession no. CAB16907, *Zea mays*, GenBank™ accession no. AI979599; *Oryza sativa*, GenBank™ accession no. AU075659; *A. thaliana*, GenBank™ accession no. AI997426; *Populus tremula*, GenBank™ accession no. AI163527; *C. elegans*, NCB accession no. CAB01233; *D. melanogaster*, GenBank™ accession no. AI512489; *Paralichthys olivaceus*, GenBank™ accession no. AU050269; *Xenopus laevis*, GenBank™ accession no. AW638624; *H. sapiens*, GenBank™ accession no. AF068754.

[3] S. G. Fox, L.-J. Tai, S. M. McFall, and R. I. Morimoto, unpublished observations.

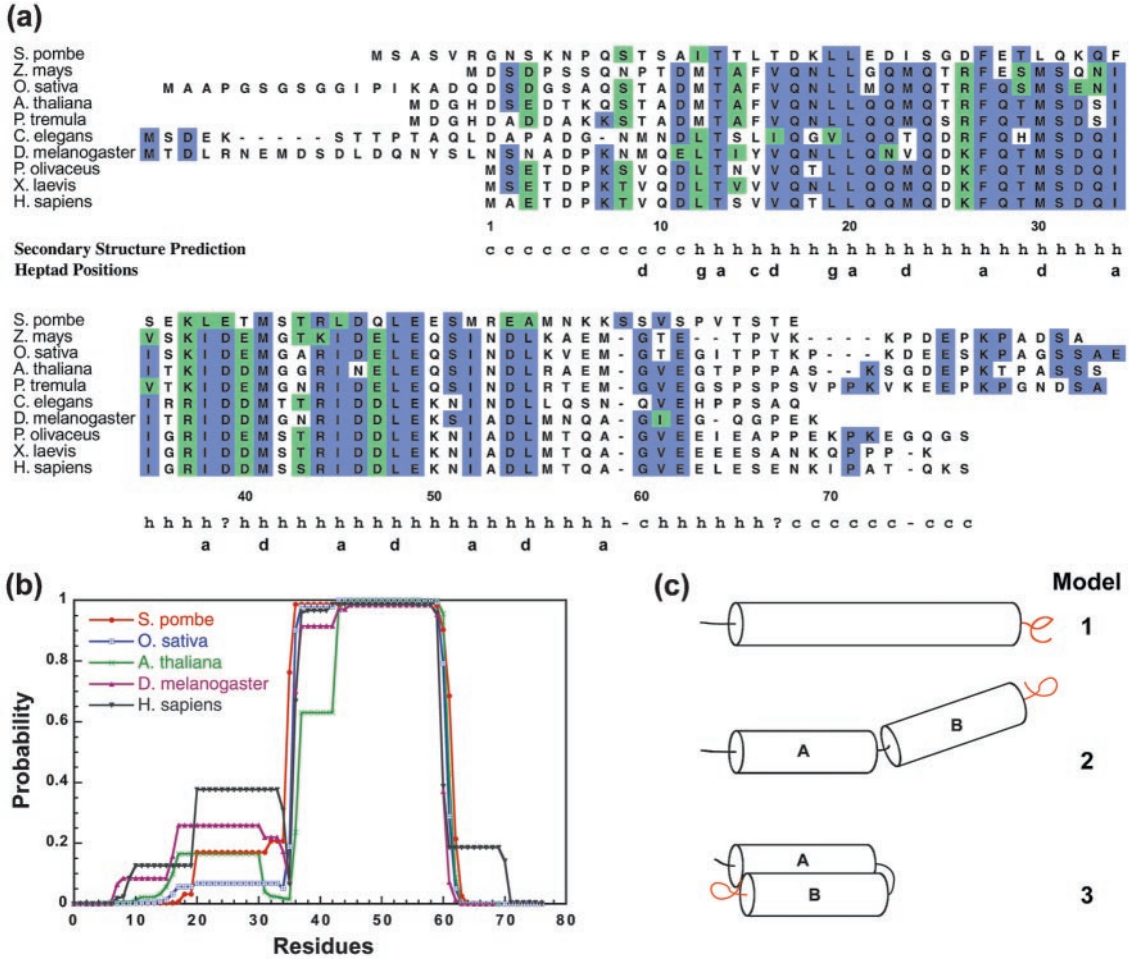

FIG. 1. **Alignment, secondary structure, and coiled-coil predictions of known and putative HSBP1 family members.** *A*, HSBP1 protein sequences from 10 species (see Footnote 2) are aligned using ClustalW. Invariant residues are shaded in blue whereas similar residues are shaded in *green*. The **a** and **d** positions of hydrophobic heptad repeats (**abcdefg**) are indicated. Residue numbering and secondary structure predictions are for the human HSBP1 sequence. *h*, helix; *c*, random coil; *?*, ambiguous assignment (Secondary Structure Consensus Prediction Program). *B*, coiled-coil predictions for five HSBP proteins using a 14-residue window (Coils 2.1). *C*, alternative structural models of HSBP1. For simplicity, helix is depicted as a *cylinder* and random coil regions are drawn as a *line*.

distortions such as breaking, bending, enhanced flexibility, or underwinding of coiled-coil structures (reviewed in Ref. 48).

We also evaluated the potential of HSBP proteins to form a coiled-coil using the computer prediction program Coils 2.1 (49). Consistent with the heptad repeat pattern assigned manually, two adjacent coiled-coil regions in the vicinity of residue 35 of human HSBP1 are predicted (Fig. 1*B*). Interestingly, HR-C has a much higher propensity to form a coiled-coil structure (>60% probability) than HR-N (10–40% probability) (Fig. 1*B*). We also assessed the potential of diverse HSBP sequences to adopt helical conformations using the Secondary Structure Consensus Prediction Program (50). Two helices are predicted in the central region, whereas random coils are predicted at the amino and carboxyl termini, coincident with the least conserved regions. The prediction is ambiguous in the vicinity of residue 39, suggesting the possibility of an unstructured "hinge" or "linker" region separating the two helices. The locations of the helices coincide largely with the hydrophobic heptad repeats (Fig. 1*A*). Collectively, our analyses suggest three alternative structural models for HSBP1 (Fig. 1*C*): 1) a single continuous helix, 2) two noninteracting helices separated by a linker region (residues 35–40), and 3) two interacting helices arranged in an anti-parallel orientation. In each of the models, the helical regions or portions thereof can engage in intermolecular interactions, giving rise to a higher order oligomer.

Human HSBP1 Is a Cooperatively Folded Protein with High Helical Content and Moderate Stability—To assess the predicted helical nature of HSBP, we performed circular dichroism (CD) studies with purified recombinant HSBP1. The CD spectrum exhibits double minima at 208 and 222 nm and a maximum near 190 nm characteristic of helical proteins (data not shown) (51). The molar ellipticity at 222 nm is indicative of a protein with a high helical content (~70%). Thermal denaturation and renaturation experiments performed by monitoring the ellipticity at 222 nm yielded two almost completely overlapping sigmoidal curves, reflecting the reversible nature of these structural transitions (data not shown). The abrupt changes in the slope of these curves near the melting temperature (48 °C) indicates that HSBP1 unfolds and refolds cooperatively, characteristic of a well folded structural unit. The thermal stability of HSBP1 is modest compared with many previously characterized coiled-coils of comparable or shorter length (8, 19, 52).

The Carboxyl Terminus of HSBP1 Is Unstructured and Accessible to Proteases—In an attempt to distinguish between contrasting structural models suggested by sequence analysis (see above), we probed the accessibility of the polypeptide backbone of HSBP1 to sequence-specific proteases. We chose two endopeptidases with different specificities: the *Staphylococcus aureus* V8 protease, which cleaves carboxyl-terminal to acidic residues (*i.e.* glutamates and aspartates), and trypsin, which cleaves carboxyl-terminal to basic residues (*i.e.* lysines and

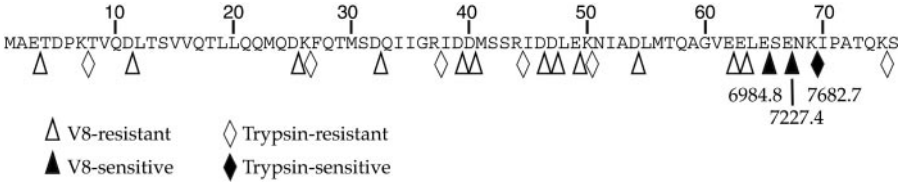

FIG. 2. **Distribution of protease-sensitive sites in HSBP1.** The *diamonds* and *triangles below* the HSBP1 sequence identify all possible cleavage sites for trypsin and V8 proteases, respectively. *Open* and *closed symbols* denote protease-resistant and protease-sensitive sites, respectively. As outlined in the text, protease-sensitive sites were deduced from the molecular mass values (indicated in Da *below* the *closed symbols*) of the proteolytic products determined by mass spectrometry.

arginines). Optimal incubation times and protein/protease ratios were determined by monitoring the disappearance of full-length protein and the appearance of proteolytic products via Western blot analyses. The proteolyzed products were then analyzed by mass spectrometry. Although V8 and trypsin proteolytic sites are uniformly distributed throughout the length of the human HSBP1 sequence, only three major products were detected (Fig. 2). V8 proteolysis produces two fragments of 6984.8 and 7227.4 daltons, whereas trypsin digestion yields a single proteolytic product of 7682.7 daltons. These fragments mapped the proteolytic cleavage sites immediately carboxyl-terminal to residues Glu-63 and Glu-65 (in the case of V8), and Lys-69 (in the case of trypsin) in the intact protein (Fig. 2).

To assess the conformational features of HSBP1 in greater detail, we recorded nuclear magnetic resonance (NMR) spectra of a uniformly ^{15}N-labeled sample at 40 °C. The ^{1}H-^{15}N heteronuclear single quantum coherence (HSQC) spectrum of HSBP1 is characterized by relatively poor signal-to-noise ratio for a majority of peaks. However, over a dozen ^{1}H-^{15}N correlations exhibit much higher than average signal intensities signifying the presence of flexible regions in the molecule (Fig. 3). These resonances were assigned from a combined analysis of three-dimensional ^{15}N-edited nuclear Overhauser effect spectroscopy (NOESY) and total correlation spectroscopy spectra. Most of the intense resonances correspond to residues at the less conserved carboxyl terminus extending approximately from Gly-60 to Ser-76. The H^{α} secondary chemical shifts and the pattern of ^{1}H-^{1}H NOEs (data not shown) further indicate the absence of regular secondary structure in this region. Thus, NMR analyses and limited proteolysis both establish that the carboxyl terminus of HSBP1 is unstructured and flexible.

HSBP1 Self-associates in Yeast Two-hybrid Interaction Assay—More detailed NMR analyses however, were impeded by the modest dispersion of amide proton resonances (characteristic of predominantly helical proteins; Fig. 3), that was further exacerbated by the presence of a large number of intense peaks arising from unstructured regions. Because intense peaks can mask less intense peaks belonging to structured regions, we designed a deletion mutant (designated HSBP1 65Δ) corresponding to residues 1–65. To establish functional equivalence of full-length HSBP1 and HSBP1 65Δ proteins and also to test whether HSBP1 can form higher-order oligomers *in vivo*, we used quantitative yeast two-hybrid interaction assays to compare the interaction strengths between the following three pairs of HSBP1 proteins: full-length HSBP1 and full-length HSBP1, full-length HSBP1 and HSBP1 65Δ, full-length HSBP1 and a truncation mutant corresponding to residue 1–45 (HSBP1 45Δ). Yeast two-hybrid assays with full-length HSBP1 as both bait and prey showed HSBP1 self-association, which was arbitrarily set to 100%. The interaction strengths were comparable between the full-length HSBP1 proteins (100%) and between full-length HSBP1 and HSBP1 65Δ (100%), whereas interaction of full-length with HSBP1 45Δ was almost completely abolished (8%). These results indicate that HSBP1 65Δ behaves identically to the full-length protein in yeast two-hybrid interaction assays and

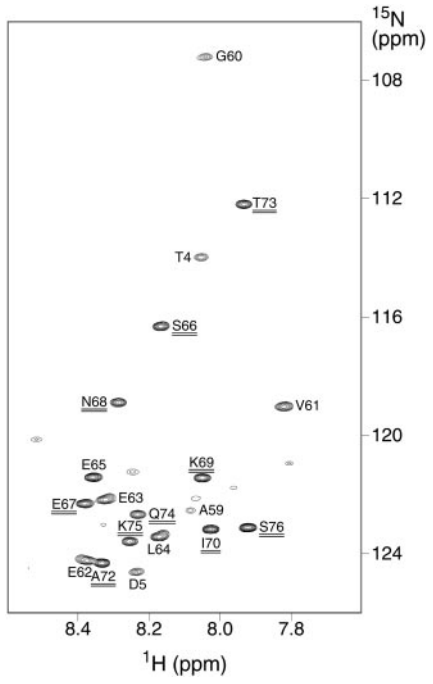

FIG. 3. **The ^{1}H-^{15}N HSQC spectrum of HSBP1.** The spectrum is contoured at a high threshold to emphasize intense correlations from flexible regions. These correlations belong to residues at the NH_2 and COOH termini. Assignments for residues 66–76 are *underlined*.

that an intact HR-C is necessary for HSBP1 self-association. Conversely, these results also suggest that the carboxyl-terminal region (residues 66–76) is not required for proper folding of the HSBP1 protein.

HSBP1 Forms a Long, Continuous Helix That Exhibits Slow Motions on the Millisecond Time Scale—The poor sensitivity of the HSQC spectra of full-length HSBP1 can be attributed to the unfavorable relaxation properties of the ^{1}H and ^{15}N spins because modified pulse sequences incorporating the TROSY effect (38) lead to remarkable improvements in both sensitivity and resolution (compare Fig. 4, *A* and *B*). The poor relaxation properties are consistent with a higher order oligomerization state and/or a highly nonglobular shape of HSBP1. Further improvements in spectral quality are seen for a ^{2}H,^{15}N-labeled sample of HSBP1 65Δ (compare Fig. 4, *B* and *C*). Significantly, the relative positions of individual resonances are virtually unchanged (except near the carboxyl terminus) in the ^{1}H-^{15}N correlated spectra of HSBP1 65Δ and full-length HSBP1, implying that the two proteins share similar structural features at concentration ranges of 500 μM to 1.6 mM.

The backbone amide proton resonances of HSBP1 polypeptides are dispersed over a 1.5 ppm range characteristic of folded proteins (Fig. 4). The somewhat modest chemical shift dispersion for amide protons is consistent with a predominantly helical conformation suggested by CD analyses. Significantly, only one set of backbone and side chain ^{1}H and ^{15}N resonances is

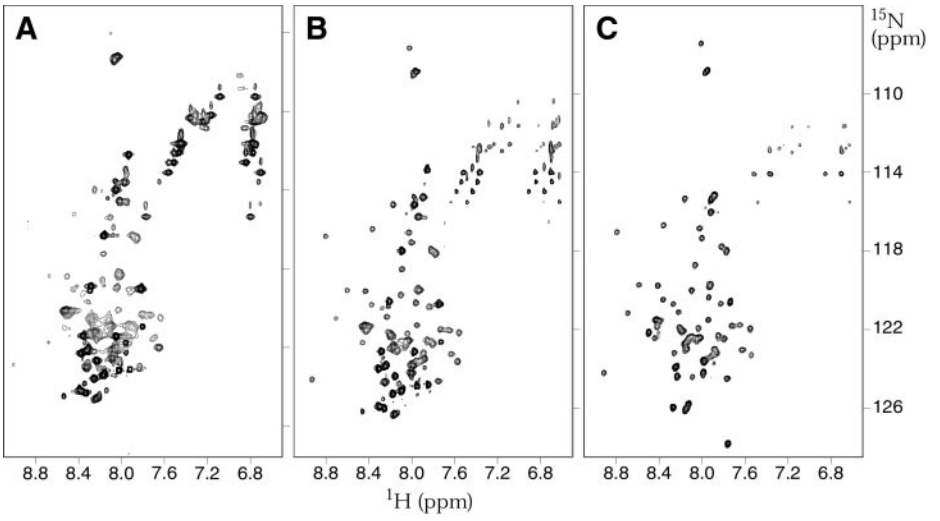

FIG. 4. **^{1}H-^{15}N correlated NMR spectra of HSBP1 and HSBP1 65Δ.** *A* and *B*, HSQC (*A*) and TROSY (*B*) spectra of a 1.6 mM uniformly ^{15}N-labeled HSBP1 sample. *C*, ^{1}H-^{15}N TROSY spectrum of a 1.3 mM uniformly ^{2}H,^{15}N-labeled HSBP1 65Δ. Experimental conditions used for these measurements are given in the text. Data were acquired, processed, and displayed using identical parameters.

detected for HSBP1, implying that each residue within a given subunit experiences an microenvironment similar to that for the corresponding residue in another subunit of a higher order oligomer.

To map the location of secondary structural elements in HSBP1, backbone $^{1}H^{N}$, ^{15}N, $^{13}C^{\alpha}$, $^{13}C^{\beta}$, and $^{13}C'$ resonances were assigned sequence-specifically by analyzing triple-resonance spectra acquired for a ^{2}H,^{13}C,^{15}N-labeled sample of HSBP1 65Δ. The $^{13}C^{\alpha}$ and $^{13}C'$ secondary chemical shifts are exquisitely sensitive probes of the local polypeptide backbone conformation (53). After applying appropriate residue-specific corrections for the deuterium isotope effect (54) to the measured values, these shifts were graphed as a function of residue number (Fig. 5, *A* and *B*). Both ^{13}C and $^{13}C'$ secondary shifts are large (>0.7 and >0.5 ppm, respectively) and positive for the polypeptide segment extending from Val-9 to Thr-57, implying a helical conformation for these residues. Sequential NOEs involving amide protons as well as medium-range $H^{\alpha}(i)$-$H^{N}(i+3)$ NOEs provide independent evidence for a helical conformation for this segment. The measured (^{1}H)-^{15}N heteronuclear NOE values (Fig. 5*C*) for this segment are also consistently large (average = 0.75 ± 0.11) and positive, implying an essentially "rigid" backbone conformation in the picosecond (ps) to nanosecond (ns) time scale. Significantly, no interruptions to these patterns (secondary chemical shift or NOE) are detected anywhere along the segment, providing direct evidence for a single continuous helix consistent with model 1 shown in Fig. 1*C*. Unfortunately, the poor sensitivity of ^{13}C-edited spectra (most likely attributable to the poor transverse relaxation properties of ^{1}H and ^{13}C spins) precluded a more detailed characterization including determination of the three-dimensional structure of HSBP1 via NMR approaches.

The surprisingly poor sensitivity of HSBP1 NMR spectra led us to quantify the spin relaxation properties of backbone ^{15}N nuclei. Spin-lattice (R_1) and spin-spin (R_2) relaxation rate constants were measured using well established approaches (40, 41). To assess any exchange contributions in the millisecond time scale, ^{15}N R_2 relaxation constants were measured as a function of the refocusing delay in the CPMG sequence (τ_{cp}). The measured R_1 and R_2 values are graphed in Fig. 6. The R_1 values are relatively small and uniform, in the helical region (residues 9–57) except near the ends, and this is reflected in the computed average and standard deviation values (0.68 ± 0.16 s^{-1}). The R_2 values are large and also uniform in the helical region (average = 11.8 ± 2.0 s^{-1} when τ_{cp} = 0.8 ms). Remarkably, a number of residues in the helical region exhibit significantly higher R_2 values when τ_{cp} is set to 5 ms. Although

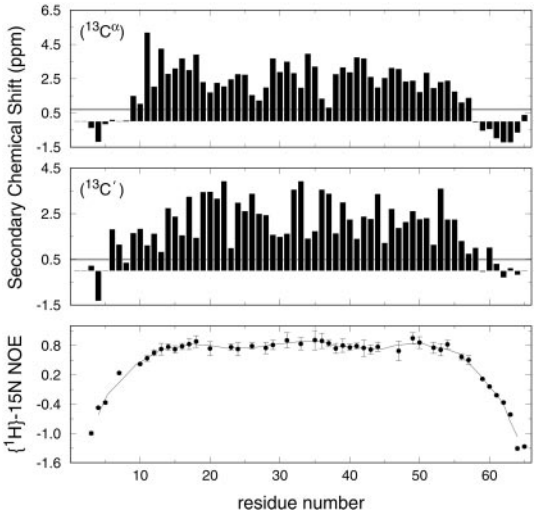

FIG. 5. **NMR analysis of secondary structure and backbone flexibility of HSBP1.** Secondary chemical shifts of α-carbon (*top panel*) and carbonyl carbon (*middle panel*) graphed as a function of residue number. The *horizontal solid gray lines* represent threshold values of 0.7 and 0.5 ppm, respectively, for an α-helix. Heteronuclear (^{1}H)-^{15}N NOEs plotted as a function of residue number (*bottom panel*). Data from a three-point smoothing function (*solid line*) are included to guide the eye.

the uncertainties in the R_2 values are higher in the latter measurement, the difference in R_2 values is clearly significant with several residues exhibiting ΔR_2 ($R_{2(\tau cp = 5\ ms)} - R_{2(\tau cp = 0.8\ ms)}$) greater than 1 s^{-1}. Qualitatively, the differences can be readily discerned from the magnetization decay curves for these residues (data not shown). Interestingly, these differences, which are indicative of motional processes occurring on the millisecond time scale, are observed for residues distributed throughout the helical region, most likely signifying some global (and possibly functionally relevant) process on this time scale.

Size Exclusion Chromatography Reveals a Discrete Molecular Species—To investigate the association properties of HSBP1, we characterized the hydrodynamic properties of the protein using size exclusion chromatography (SEC). Experiments were performed with loading concentrations ranging from 5 to 500 μM and under a variety of ionic and pH conditions (Fig. 7 and data not shown). In each case, HSBP1 eluted as a single peak with an apparent molecular mass of 62.4 ± 3.7 kDa, which is much larger than the calculated monomeric molecular mass of 8.4 kDa. The symmetry of the peak further

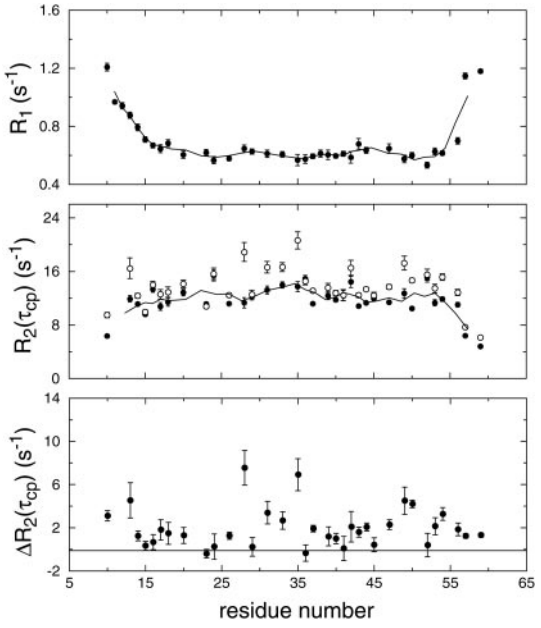

FIG. 6. **Measured spin relaxation parameters of backbone ^{15}N nuclei of HSBP1 at 14.1 T.** Spin-lattice R_1 (*top panel*) and spin-spin R_2 (*middle panel*) relaxation rate constants graphed as a function of residue number. Data from a three-point smoothing function (*solid line*) is included to guide the eye. R_2 measurements performed using CPMG refocusing delays (τ_{cp}) of 0.8 ms (*filled symbols*) and 5 ms (*open symbols*). The difference in the measured R_2 ($\Delta R_2 = R_{2(\tau cp = 5\ ms)} - R_{2(\tau cp = 0.8\ ms)}$) values is graphed in the *bottom panel*.

suggests a discrete molecular species under these conditions. The elution profile is very similar to that of bovine serum albumin (Fig. 7), which is a 66.4-kDa globular protein. This suggests that HSBP1 either forms a large oligomer and/or has a highly nonglobular shape that contributes to increased surface area and frictional properties of the protein.

HSBP1 Exists as Mixture of Trimer and Hexamer in Native Gels—To further establish the oligomerization state of HSBP1, we took advantage of the different sizes of purified wild-type and HSBP1 65Δ proteins. A mixture of wild-type and HSBP1 65Δ was incubated to allow formation of homo- and hetero-oligomers that were then resolved on a nondenaturing gel. The number of discrete species detected is expected to follow a binomial distribution, $(A+B)^n$, where n corresponds to the oligomerization state of the protein which determines the number of bands ($n + 1$) on the gel (55–57). For example, for a trimeric protein, four discrete bands would be detected in a nondenaturing gel. Discrete bands with substantially different mobilities were observed for both wild-type and HSBP1 65Δ, presumably because of size and pI differences (Fig. 8, compare *lanes 1* and *2*, *lanes 4* and *5*, and *lanes 7* and *8*). On a 12% acrylamide native gel, four bands were observed, indicating the presence of homotrimers, $(\text{wild-type})_3$ and $(\text{HSBP1 65}\Delta)_3$, as well as two types of heterotrimers with intermediate mobilities, $(\text{wild-type})_2(\text{HSBP1 65}\Delta)_1$ and $(\text{wild-type})_1(\text{HSBP1 65}\Delta)_2$ (Fig. 8, *lane 3*). Variation in the time and temperature of incubation of the two HSBP1 proteins yielded very similar results (data not shown). Interestingly, hetero-oligomers were detected after only 5 min of co-incubation at room temperature. Although native gel analyses are not well suited for measuring association/dissociation kinetics because of the long dead times in loading and running gels, this result suggests that the kinetics of exchange between subunits of the oligomer is relatively rapid, although thermodynamically, the oligomeric state is clearly more preferred.

Intriguingly, at very high protein loading concentrations and/or at much longer film exposure time following enhanced chemiluminescence, less intense and closely spaced bands with slower mobilities could be observed (Fig. 8, *lane 6*). The number of discrete bands could not be readily determined, partly because of the intense bands from the trimeric species. By varying the temperature, buffer, and the percentage of acrylamide in the resolving gel, we found conditions where these less intense bands in the 12% acrylamide gels constituted the major species in 8–10% acrylamide gradient gels. A cluster of seven discrete bands could be readily observed in these gels, demonstrating the existence of hexamers (Fig. 8, *lanes 7–9*). On an 8–12% gradient gel, however, the relative intensities of the bands from the hexameric and trimeric species are equivalent (data not shown). Collectively, these results suggest that the percentage of acrylamide in the gel plays a role in influencing the oligomeric state of HSBP1. Although it is presently unclear how pore size of the gel affects HSBP1 oligomerization, native gel analyses clearly demonstrate that HSBP1 can exist either as a trimer or a hexamer.

HSBP1 Exists in a Trimer-Hexamer Equilibrium in Analytical Ultracentrifugation—In contrast to native gel analyses, SEC measurements had indicated the presence of a single molecular species of HSBP1 (see above). To resolve this apparent discrepancy and to assess the relative populations of trimers and hexamers (if any), sedimentation velocity experiments on an analytical ultracentrifuge were performed with samples in the monomeric concentration range from 5 to 1000 μM (58). Sedimentation velocity data were initially analyzed with the model-independent van Holde-Weischet method (45). These analyses revealed the presence of multiple species correlating to the loading concentration (59) (Fig. 9). Between 10 and 100 μM loading concentration, HSBP1 sediments as a single 1.8–2.2 S species. At 5 μM loading concentration, the dominant species has a sedimentation coefficient of ~2 S, whereas smaller and heterogeneous sedimentation coefficients are seen at the lowest protein concentration boundaries, consistent with a complex dissociating into smaller subunits. Similarly at 500 μM, ~70% of the population sediments as a ~2 S species, whereas HSBP1 proteins at the more concentrated fractions have higher sedimentation coefficients (up to 2.7 S), possibly indicative of the presence of higher order oligomers. At the highest loading concentration studied (1000 μM), a concentration-dependent decrease of the sedimentation coefficient is observed, characteristic of nonideal behavior. Nonideal effects can be attributed to high concentration, unusual charge distribution, highly asymmetric and nonglobular shape, or large size (59, 60). For HSBP1, the first three factors probably contribute significantly toward nonideality because the protein is highly acidic (calculated pI = 4.2) and has a highly unusual shape given that the protein is dominated by a rather long, continuous helix (see below).

Sedimentation velocity data measured at 100 μM loading concentration were also analyzed using the finite element analysis approach to gain insights into the molecular size of HSBP1 (46, 61). The data were fitted to a single component system, which resulted in a molecular mass of 25.7 kDa for the ~2 S species, consistent with trimeric HSBP1 at most concentrations studied (5–500 μM). Finite element analysis further revealed a highly nonglobular shape for the HSBP1 trimer, with a Perrin shape factor f/f_0 ratio of ~1.57 (Table I). Modeling HSBP1 as a prolate ellipsoid, we estimate the lengths of the minor and major axes to be 8.9 Å by 93.2 Å, respectively (62). The estimated length is much longer than what would be expected for a 49-residue α-helix (~75 Å), which suggests that the unstructured regions at the NH_2 and COOH termini contribute significantly to the apparent length. Because HSBP1

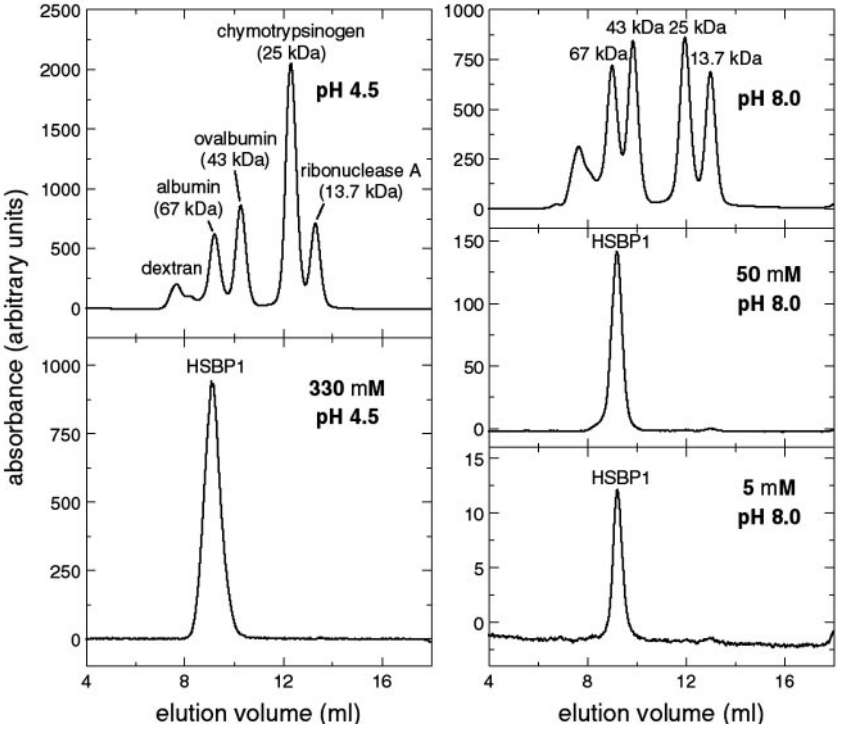

FIG. 7. **High resolution size exclusion chromatography analysis of HSBP1.** These measurements were conducted in pH 8 or pH 4.5 buffer at 23.5 °C. HSBP1 starting concentrations ranged from 5 to 330 μM. Details of the solution conditions are given in the text. The protein standards used are albumin (mass, 67 kDa; Stokes radius, 36.1 Å), ovalbumin (43 kDa, 27.6 Å), chymotrypsinogen (25 kDa, 22.5 Å), and ribonuclease A (13.7 kDa, 18 Å).

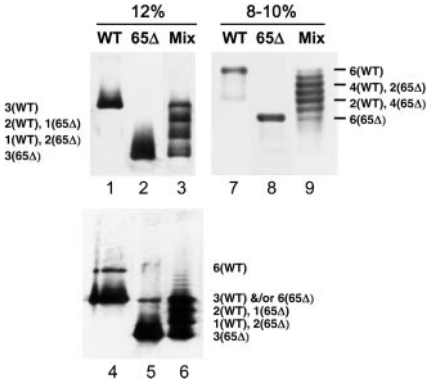

FIG. 8. **Nondenaturing gels of HSBP1 and HSBP1 65Δ.** *Lanes 1–6* are from a 12% acrylamide gel, whereas *lanes 7–9* are from an 8–10% gradient gel. Labels at the *top* of the *lanes* denote sample component(s) (*WT*, HSBP1; *65*Δ, HSBP1 65Δ; *Mix*, 1:1 mixture of HSBP1 and HSBP1 65Δ). 1 μg of total protein was loaded in each lane for *lanes 4–6*, which was 20 times the amount loaded in the other lanes. Both homotrimers and homohexamers can be readily detected in *lanes 4* and *5*. However, only some of the bands most likely corresponding to heterohexamers can be observed in *lane 6*. In *lane 9*, the labels for heterohexamers 5(wild-type)1(65Δ), 3(wild-type)3(65Δ), and 1(wild-type)5(65Δ) have been omitted for clarity.

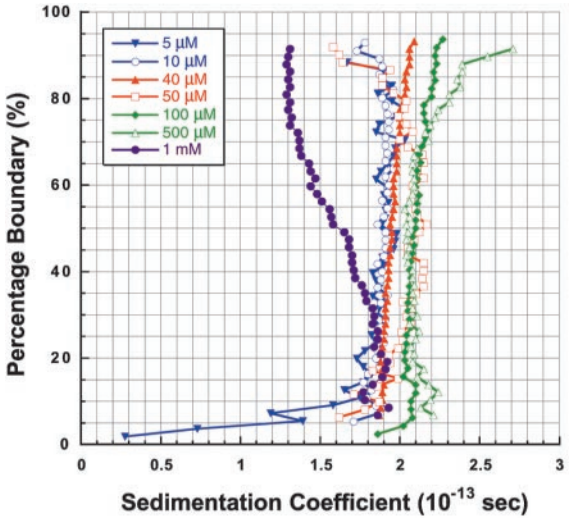

FIG. 9. **Sedimentation velocity analysis of HSBP1.** van Holde-Weischet integral distribution plots (boundary fraction *versus* $s_{20,w}$) were derived from sedimentation velocity experiments of HSBP1. Starting concentrations of the HSBP1 samples ranged from 5 μM to 1 mM. The wavelengths at which data were obtained were 210 nm for 5 μM, 220 nm for 10 μM, 236 nm for 50 μM, 240 nm for 100 μM, 246 nm for 500 μM, and 248 nm for 1 mM. Starting absorbance ranged between 0.3 and 0.6.

concentrations employed for the NMR and SEC studies were close to the range used for sedimentation velocity studies, we also conclude that the species in NMR and SEC measurements corresponds to the trimeric form of HSBP1. The nonglobular shape probably contributes toward the anomalous elution profile of HSBP1 as a 62-kDa protein in SEC and also to the poor nuclear spin relaxation properties of HSBP1.

In summary, we deduce from sedimentation velocity analyses single trimeric species at most concentrations examined, minor and smaller species at concentrations well below 5 μM, a trimer ↔ hexamer equilibrium above 500 μM, and nonideality at 1 mM starting concentration. Two distinct boundaries corresponding to the trimeric and hexameric species were not observed in the 500 μM experiment, indicating that either the interconversion between the two species is rapid or the sedimentation coefficients are very similar (62), or that there exist multiple equilibria between trimers, hexamers, and small amounts of higher order oligomers.

To determine the oligomerization state of HSBP1 independent of shape considerations, we performed sedimentation equilibrium studies at multiple loading concentrations (ranging from 10 to 26 μM) and speed (15,000–50,000 rpm). Seventeen equilibrium scans were fitted globally using UltraScan 5.0 software (B. D.) to an ideal single-component model, and self-associating multicomponent models including the monomer ↔ dimer, monomer ↔ dimer ↔ trimer, monomer ↔ dimer ↔ tetramer models. The monomer ↔ dimer model was found to be the most satisfactory model for describing the data, and it resulted in random residuals and a monomeric molecular mass

TABLE I

Hydrodynamic parameters derived from sedimentation velocity data

The data measured at 100 μM loading concentration were fitted to a single component system using the finite element analysis approach to determine the molecular weight of HSBP1 and to estimate the dimension of the molecule. Sedimentation coefficients, diffusion coefficients, and molecular mass values were corrected for water at 20 °C as reported by UltraScan.

Variance	5.28799×10^{-5}
No. of fitted parameters	4
No. of fitted data points	28,830
Molecular mass (fitted)	25.7 kDa
Sedimentation coefficient ($s_{20,w}$) (fitted)	2.03×10^{-13} *s*
Translational diffusion coefficient ($D_{20,w}$) (fitted)	7.02×10^{-7} *D*
Loading concentration (fitted)	0.374 OD_{240}
V_{bar} (corrected for 20 °C) (fixed)	0.7274 ml/g
Radius of minimal sphere	19.5 Å
Radius of Stoke's sphere	32.0 Å
Frictional coefficient	5.76×10^{-8}
Minimal sphere f_0	3.68×10^{-8}
Frictional ratio (f/f_0)	1.57
Volume of molecule	30.9×10^2 Å^3
	Hydrodynamic model (assume prolate ellipsoid)
Axial ratios	10.5
Length of semi-major axis	93.2 Å
Length of semi-minor axis	8.9 Å

of 23.1 ± 0.3 kDa (data not shown). The deduced molecular mass closely matches the computed molecular weight for trimeric HSBP1, indicative of a self-associating trimer ↔ hexamer system. The complexity of this system, as revealed by sedimentation velocity studies, however, precluded quantitative analysis of the association constants. We therefore conclude that the principal species detected in sedimentation velocity and equilibrium experiments is the trimeric form of HSBP1.

DISCUSSION

The results of our biophysical and biochemical analyses led us to propose a structural model for HSBP1 illustrated in Fig. 10. According to this model, HSBP1 consists of a single and continuous α-helical region (~49 residues) with unstructured regions at the amino and carboxyl termini. The helical regions associate in a parallel and unstaggered manner to form a coiled-coil trimer of a highly elongated shape. HSBP1 is unusual in that, unlike many proteins, the protein appears to be characterized by only a single structural feature, namely a coiled-coil trimerization domain.

The coiled-coil region is highly conserved, and the high degree of sequence conservation across the entire HSBP family suggests that the biophysical properties described herein for human HSBP1 are likely to be relevant to other members of the family. It also suggests the importance of the conserved coiled-coil domain to HSBP function. For the heptad repeat regions to form coiled-coils, the overall sequence can diverge as long as similarly sized hydrophobic residues are located at the **a** and **d** positions to ensure packing of the interhelical space. Thus, the sequence conservation of HSBP suggests that the helical region may have other purposes in addition to self-association. Furthermore, it is likely that protein domains that interact with HSBP will also be highly conserved because of co-evolution. Although HSBP1 was originally identified through its interaction with HSF1 trimerization domain in the yeast two-hybrid essay, the HSF1 trimerization domain is comparatively more divergent. (Sequence similarity between HSF1 trimerization domain across plant and animal kingdoms is ~30% (Ref. 63); in contrast, sequence similarity between HSBP1 trimerization domain across plant and animal kingdoms is more than 65%.)

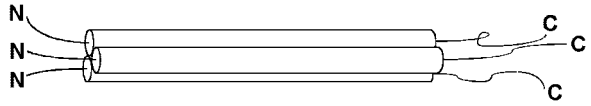

FIG. 10. **A structural model for the HSBP1 trimer.** The amino-terminal 8 residues and the carboxyl-terminal 19 residues are depicted as *curved lines* to imply that these regions are unstructured. The cylinders correspond to helical regions formed by the central 49-residue segment, which functions as the oligomerization domain.

This suggests that HSBP1 may interact with proteins other than the trimerization domain of HSF1 in the cell.

The fact that HSBP1 forms a continuous helix and is a trimer strongly suggests that both HR-N and HR-C participate in coiled-coil interactions. However, the coiled-coil prediction based on protein sequence data suggests that HR-N has a relatively low probability to form a coiled-coil and that the helical region of HSBP1 may not be continuous (Fig. 1). We suggest that this discrepancy results from the presence of consecutive hydrophobic residues in the first two heptads of HR-N and the presence of a conserved threonine residue at the **a** position of the first repeat. Hydrophobic amino acids at the **c** and **g** positions in HR-N dictate that some of the hydrophobic residues are exposed to the solvent and capable of providing additional hydrophobic interacting surface for competing oligomerization states. Indeed when the hydrophobic residues at the **g** and **c** positions were changed to hydrophilic residues, the predicted probability for coiled-coil formation increased substantially (from 30% to >50%). Additionally replacing the threonine, which is not commonly found at the **a** position in coiled-coils (49) with a leucine increases the probability even further (to 80%). These results indicate that, although the heptad repeat appears to be a relatively simple motif and has been extensively studied, there are complexities (for review, see Ref. 64) dictating the formation of coiled-coils that are not well understood. Studies of HSBP1 protein family could thus provide new insights into the relationship between protein sequence and coiled-coil structure and function and allow more reliable predictions.

Although the 49-residue helical region (corresponding to ~14 helical turns) of HSBP1 implies a fairly extensive coiled-coil interface in the HSBP1 trimer, the protein exhibits surprisingly modest thermal stability (T_m ~50 °C), comparable with that of the zipper region (~10 helical turns) of dimeric basic leucine zipper transcription factors (65), but in marked contrast to the tetrameric soluble *N*-ethylmaleimide-sensitive factor attachment protein receptor complex (~17 helical turns and T_m >90 °C) (66). A survey of previously characterized coiled-coils, however, reveals no correlation between helix length and thermal stability. Many structural proteins, including myosin, contain relatively long coiled-coil domains (in excess of 600 residues) but have relatively low melting temperatures (T_m between 40 and 50 °C) (67, 68). Thus, although the coiled-coil domain of HSBP1 is similar in length to that of many proteins involved in transcriptional activation and signal transduction, unlike these domains, its thermal stability is comparatively lower and resembles that of the coiled-coil domains of structural proteins.

Another remarkable feature of the HSBP1 protein, possibly related to its modest thermal stability, is the prevalence of motional processes on the millisecond time scale particularly in the coiled-coil region. Interestingly, the polypeptide backbone in this region appears to be relatively rigid on the picosecond to nanosecond time scale as indicated by the uniformly large (^{1}H)-^{15}N NOE values. Although previous studies of basic leucine zipper domain of GCN4 implicate motional processes on picosecond/nanosecond time scale in the DNA-binding domain immediately adjacent to the coiled-coil region (69), slower time

scale processes in the coiled-coil region are not apparent. The coiled-coil region of HSBP1 thus appears to be unique in this regard. Although the origin of the slower motional processes is presently unknown, we note the rapid subunit exchange between HSBP1 oligomers within minutes of incubation in our native gel studies, as well as the rapid exchange of oligomerization states implied by sedimentation velocity data (500 μM, Fig. 9). Indeed, we note a striking parallel with the Fos-Jun heterodimer, which exhibits rapid dissociation kinetics in the absence of cognate DNA but not when the AP-1 DNA binding site is present (70). Thus, dynamic motions in the millisecond time scale observed in the coiled-coil region of HSBP1 may be coupled to its biological function.

The fact that human HSBP1 has only one readily recognizable structural motif suggests that it functions most likely by associating with other proteins through coiled-coil interactions. Whether it interacts through the same residues that are involved in stabilizing the trimer or through an entirely different surface remains to be explored. The former possibility, which involves dissociation of the trimer into individual subunits is attractive because the kinetics of subunit exchange deduced qualitatively from native gel analyses is relatively rapid (*i.e.* on the minute time scale). The second possibility, which involves formation of a higher order oligomeric complex with the HSBP trimer, cannot be ruled out because the HR-N region contains multiple, conserved hydrophobic residues at the **c** and **g** positions that can mediate specific association with other proteins. A particularly well characterized example of this type of interaction involving a homotrimer has been described for hemagglutinin, a glycoprotein of the influenza virus (71). Although the degree of sequence conservation at the NH_2 and COOH termini is low (Fig. 1), we cannot formally exclude the possibility of these regions being involved in some aspect of protein function.

Our biophysical and biochemical characterization of HSBP1 constitutes the first step toward defining the functional properties of this novel protein family. Unlike other coiled-coil proteins in which the oligomerization domain functions in concert with other domains, such as during transcriptional activation or signal transduction, HSBP1 appears to function solely through protein oligomerization perhaps to regulate the function of other proteins. Additional studies are required to clarify the role of HSBP in the cell, but it is expected that the structural and dynamical features of this protein describe herein will be particularly important for designing experiments and interpreting results that will lead to a better understanding of the mechanism of regulation via coiled-coil interactions in general, and this evolutionarily conserved protein in particular.

Acknowledgments—We are most grateful to Professor Jon Widom for invaluable advice. We thank Professor Susan K. Pierce and Julie Kim for assistance and advice with monoclonal antibody production, and Reiko Yamada for assistance with protein production. We also thank Professors Rick Gaber and Roger Brent for providing expression constructs, as well as Professor Ted Jardetzky for critical reading of the manuscript. We gratefully acknowledge the use of instruments at the Keck Biophysics Facility at Northwestern and Dr. Kate Spiegel, Andrew Murphy, and Joshua Hays for technical assistance (www.biochem.northwestern.edu/Keck/keckmain.html).

REFERENCES

1. Lupas, A. (1996) *Trends Biochem. Sci.* **21,** 375–382
2. Beck, K., and Brodsky, B. (1998) *J. Struct. Biol.* **122,** 17–29
3. Geisler, N., Kaufmann, E., and Weber, K. (1982) *Cell* **30,** 277–286
4. Sheriff, S., Chang, C. Y., and Ezekowitz, R. A. (1994) *Nat. Struct. Biol.* **1,** 789–794
5. O'Shea, E. K., Rutkowski, R., Stafford, W. F., III, and Kim, P. S. (1989) *Science* **245,** 646–648
6. Rabindran, S. K., Haroun, R. I., Clos, J., Wisniewski, J., and Wu, C. (1993) *Science* **259,** 230–234
7. Sarge, K. D., Murphy, S. P., and Morimoto, R. I. (1993) *Mol. Cell. Biol.* **13,** 1392–1407
8. Lumb, K. J., Carr, C. M., and Kim, P. S. (1994) *Biochemistry* **33,** 7361–7367
9. Monera, O. D., Zhou, N. E., Kay, C. M., and Hodges, R. S. (1993) *J. Biol. Chem.* **268,** 19218–19227
10. Yang, P. K., Tzou, W. S., and Hwang, M. J. (1999) *Biopolymers* **50,** 667–677
11. Nautiyal, S., and Alber, T. (1999) *Protein Sci.* **8,** 84–90
12. Ogihara, N. L., Weiss, M. S., Degrado, W. F., and Eisenberg, D. (1997) *Protein Sci.* **6,** 80–88
13. Crick, F. H. C. (1953) *Acta Crystallogr.* **6,** 689–697
14. O'Shea, E. K., Klemm, J. D., Kim, P. S., and Alber, T. (1991) *Science* **254,** 539–544
15. Harbury, P. B., Zhang, T., Kim, P. S., and Alber, T. (1993) *Science* **262,** 1401–1407
16. Potekhin, S. A., Medvedkin, V. N., Kashparov, I. A., and Venyaminov, S. (1994) *Protein Eng.* **7,** 1097–1101
17. Kohn, W. D., Monera, O. D., Kay, C. M., and Hodges, R. S. (1995) *J. Biol. Chem.* **270,** 25495–25506
18. Lumb, K. J., and Kim, P. S. (1995) *Science* **268,** 436–439
19. Gonzalez, L., Jr., Woolfson, D. N., and Alber, T. (1996) *Nat. Struct. Biol.* **3,** 1011–1018
20. Gonzalez, L., Jr., Brown, R. A., Richardson, D., and Alber, T. (1996) *Nat. Struct. Biol.* **3,** 1002–1009
21. Monera, O. D., Sönnichsen, F. D., Hicks, L., Kay, C. M., and Hodges, R. S. (1996) *Protein Eng.* **9,** 353–363
22. Zeng, X., Herndon, A. M., and Hu, J. C. (1997) *Proc. Natl. Acad. Sci. U. S. A.* **94,** 3673–3678
23. Fasshauer, D., Sutton, R. B., Brünger, A. T., and Jahn, R. (1998) *Proc. Natl. Acad. Sci. U. S. A.* **95,** 15781–15786
24. Kohn, W. D., Kay, C. M., and Hodges, R. S. (1998) *J. Mol. Biol.* **283,** 993–1012
25. Wagschal, K., Tripet, B., and Hodges, R. S. (1999) *J. Mol. Biol.* **285,** 785–803
26. Wagschal, K., Tripet, B., Lavigne, P., Mant, C., and Hodges, R. S. (1999) *Protein Sci.* **8,** 2312–2329
27. Tripet, B., Wagschal, K., Lavigne, P., Mant, C. T., and Hodges, R. S. (2000) *J. Mol. Biol.* **300,** 377–402
28. Satyal, S. H., Chen, D., Fox, S. G., Kramer, J. M., and Morimoto, R. I. (1998) *Genes Dev.* **12,** 1962–1974
29. Ausubel, F. M., Brent, R., Kingston, R. E., Moore, D. D., Seidman, J. G., Smith, J. A., and Struhl, K. (1998) in *Current Protocols in Molecular Biology* (Chanda, V. B., ed) Vol. 4, pp. 20.1.1–20.1.40, John Wiley & Sons, Inc., New York
30. Miller, J. H. (1972) *Experiments in Molecular Genetics*, pp. 352–355, Cold Spring Harbor Laboratory Press, Cold Spring Harbor, NY
31. Harlow, E., and Lane, D. (1988) *Antibodies: A Laboratory Manual*, pp. 53–282, Cold Spring Harbor Laboratory Press, Cold Spring Harbor, NY
32. Chen, Y. H., Yang, J. T., and Martinez, H. M. (1972) *Biochemistry* **11,** 4120–4131
33. Cai, M., Huang, Y., Sakaguchi, K., Clore, G. M., Gronenborn, A. M., and Craigie, R. (1998) *J. Biomol. NMR* **11,** 97–102
34. Radhakrishnan, I., Perez-Alvarado, G. C., Parker, D., Dyson, H. J., Montminy, M. R., and Wright, P. E. (1999) *J. Mol. Biol.* **287,** 859–865
35. Muhandiram, D. R., and Kay, L. E. (1994) *J. Magn. Reson.* **103,** 203–216
36. Yamazaki, T., Lee, W., Arrowsmith, C. H., Muhandiram, D. R., and Kay, L. E. (1994) *J. Am. Chem. Soc.* **116,** 11655–11666
37. Zhu, G., Kong, X. M., and Sze, K. H. (1999) *J. Biomol. NMR* **13,** 77–81
38. Pervushin, K., Riek, R., Wider, G., and Wüthrich, K. (1997) *Proc. Natl. Acad. Sci. U. S. A.* **94,** 12366–12371
39. Weigelt, J. (1998) *J. Am. Chem. Soc.* **120,** 10778–10779
40. Farrow, N. A., Muhandiram, R., Singer, A. U., Pascal, S. M., Kay, C. M., Gish, G., Shoelson, S. E., Pawson, T., Forman-Kay, J. D., and Kay, L. E. (1994) *Biochemistry* **33,** 5984–6003
41. Loria, J. P., Rance, M., and Palmer, A. G., III (1999) *J. Biomol. NMR* **15,** 151–155
42. Palmer, A. G., III, Rance, M., and Wright, P. E. (1991) *J. Am. Chem. Soc.* **113,** 4371–4380
43. Laue, T. M., and Rhodes, D. G. (1990) *Methods Enzymol.* **182,** 566–587
44. Ausubel, F. M., Brent, R., Kingston, R. E., Moore, D. D., Seidman, J. G., Smith, J. A., and Struhl, K. (1998) in *Current Protocols in Molecular Biology* (Chanda, V. B., ed) Vol. 2, pp. 10.2A.1–10.3.35, John Wiley & Sons, Inc., New York
45. van Holde, K. E., and Weischet, W. O. (1978) *Biopolymers* **17,** 1387–1403
46. Demeler, B., and Saber, H. (1998) *Biophys. J.* **74,** 444–454
47. Altschul, S. F., Madden, T. L., Schaffer, A. A., Zhang, J., Zhang, Z., Miller, W., and Lipman, D. J. (1997) *Nucleic Acids Res.* **25,** 3389–3402
48. Brown, J. H., Cohen, C., and Parry, D. A. (1996) *Proteins* **26,** 134–145
49. Lupas, A., Van Dyke, M., and Stock, J. (1991) *Science* **252,** 1162–1164
50. Deleage, G., Blanchet, C., and Geourjon, C. (1997) *Biochimie* (*Paris*) **79,** 681–686
51. Chen, Y.-H., Yang, J. T., and Chau, K. H. (1974) *Biochemistry* **13,** 3350–3359
52. Steinmetz, M. O., Stock, A., Schulthess, T., Landwehr, R., Lustig, A., Faix, J., Gerisch, G., Aebi, U., and Kammerer, R. A. (1998) *EMBO J.* **17,** 1883–1891
53. Wishart, D. S., and Sykes, B. D. (1994) *Methods Enzymol.* **239,** 363–392
54. Venters, R. A., Farmer, B. T., II, Fierke, C. A., and Spicer, L. D. (1996) *J. Mol. Biol.* **264,** 1101–1116
55. Cantor, C. R., and Schimmel, P. R. (1980) *The Biophysical Chemistry,* Vol. 1, p. 137, W. H. Freeman, San Francisco
56. Hope, I. A., and Struhl, K. (1987) *EMBO J.* **6,** 2781–2784
57. Sorger, P. K., and Nelson, H. C. (1989) *Cell* **59,** 807–813
58. Carruthers, L. M., Schirf, V. R., Demeler, B., and Hansen, J. C. (2000) *Methods Enzymol.* **321,** 66–80
59. Demeler, B., Saber, H., and Hansen, J. C. (1997) *Biophys. J.* **72,** 397–407
60. Ralston, G. B. (1993) *Introduction to Analytical Ultracentrifugation*, p. 21, Beckman Instruments, Inc., Fullerton, CA
61. Demeler, B., Behlke, J., and Ristau, O. (2000) *Methods Enzymol.* **321,** 38–65
62. Cantor, C. R., and Schimmel, P. R. (1980) *The Biophysical Chemistry,* Vol. 2,

W. H. Freeman, San Francisco
63. Wu, C. (1995) *Annu. Rev. Cell Dev. Biol.* **11,** 441–469
64. Lupas, A. (1997) *Curr. Opin. Struct. Biol.* **7,** 388–393
65. O'Shea, E. K., Rutkowski, R., and Kim, P. S. (1992) *Cell* **68,** 699–708
66. Fasshauer, D., Eliason, W. K., Brünger, A. T., and Jahn, R. (1998) *Biochemistry* **37,** 10354–10362
67. Zolkiewski, M., Redowicz, M. J., Korn, E. D., Hammer, J. A., and Ginsburg, A. (1997) *Biochemistry* **36,** 7876–7883
68. King, L., Seidel, J. C., and Lehrer, S. S. (1995) *Biochemistry* **34,** 6770–6774
69. Bracken, C., Carr, P. A., Cavanagh, J., and Palmer, A. G., III (1999) *J. Mol. Biol.* **285,** 2133–2146
70. Patel, L. R., Curran, T., and Kerppola, T. K. (1994) *Proc. Natl. Acad. Sci. U. S. A.* **91,** 7360–7364
71. Wilson, I. A., Skehel, J. J., and Wiley, D. C. (1981) *Nature* **289,** 366–373